ACS Catalysis

Albright COLLEGE

Subscriber access provided by ALBRIGHT COLLEGE

Article

Dissecting the performance of nanoporous gold catalysts for oxygen-assisted coupling of methanol with fundamental mechanistic and kinetic information

Christian Reece, Mathilde Luneau, and Robert J. Madix

ACS Catal., **Just Accepted Manuscript** • DOI: 10.1021/acscatal.9b00664 • Publication Date (Web): 09 Apr 2019

Downloaded from http://pubs.acs.org on April 11, 2019

Just Accepted

"Just Accepted" manuscripts have been peer-reviewed and accepted for publication. They are posted online prior to technical editing, formatting for publication and author proofing. The American Chemical Society provides "Just Accepted" as a service to the research community to expedite the dissemination of scientific material as soon as possible after acceptance. "Just Accepted" manuscripts appear in full in PDF format accompanied by an HTML abstract. "Just Accepted" manuscripts have been fully peer reviewed, but should not be considered the official version of record. They are citable by the Digital Object Identifier (DOI®). "Just Accepted" is an optional service offered to authors. Therefore, the "Just Accepted" Web site may not include all articles that will be published in the journal. After a manuscript is technically edited and formatted, it will be removed from the "Just Accepted" Web site and published as an ASAP article. Note that technical editing may introduce minor changes to the manuscript text and/or graphics which could affect content, and all legal disclaimers and ethical guidelines that apply to the journal pertain. ACS cannot be held responsible for errors or consequences arising from the use of information contained in these "Just Accepted" manuscripts.

ACS Publications

is published by the American Chemical Society. 1155 Sixteenth Street N.W., Washington, DC 20036

Published by American Chemical Society. Copyright © American Chemical Society. However, no copyright claim is made to original U.S. Government works, or works produced by employees of any Commonwealth realm Crown government in the course of their duties.

Dissecting the Performance of Nanoporous Gold Catalysts for Oxygen-Assisted Coupling of Methanol with Fundamental Mechanistic and Kinetic Information

Christian Reece[1], Mathilde Luneau[1], and Robert. J. Madix[2*]

1. Harvard University, Department of Chemistry and Chemical Biology, Cambridge, MA, 02138 USA
2. Harvard University, School of Engineering and Applied Science, Cambridge, MA, 02138 USA

*corresponding author: rmadix@seas.harvard.edu

Abstract

The utility of the surface reactivity observed for model systems under ultra-high vacuum for predicting the performance of catalytic materials under ambient flow conditions is a highly debated topic in heterogeneous catalysis. Herein we show that vast differences in selectivity observed for methanol self-coupling across wide ranges of temperature and reactant pressure can be accurately predicted utilising the kinetics and mechanism obtained from model studies on gold single crystals in ultrahigh vacuum regressed to fit transient pulse responses over nanoporous gold ($Ag_{0.03}Au_{0.97}$) at low pressures (TAP). Specifically, microkinetic modelling of the complex sequence of elementary steps governing this reaction predicts the dramatic effect of reactant partial pressure on the product distribution and leads to conclusion that the gas phase partial pressures of both reactants and the reaction temperature determine the changes in selectivity to methyl formate formation. Moreover, thorough analysis of the reaction network indicates that the product distribution becomes increasingly insensitive to kinetic effects at pressures approaching 1 bar, leading toward 100% selectivity methyl formate. A rigorous kinetic sensitivity analysis also demonstrates the complex interplay of the kinetics of the elementary steps and the overall catalytic behaviour.

Keywords:

Catalysis, Kinetics, Alcohols, Esters, Physical Chemistry, Chemical Engineering

1. Introduction

With the ever-increasing demand for more energy efficient and selective catalysts there is a strong drive to develop techniques and methods which can be used to understand reaction networks and catalytic systems at the microkinetic and molecular level. For the past half century, two cornerstones of heterogenous catalytic research have been precise, fundamental measurements taken on model systems under ultra-high vacuum (UHV) conditions and reactor studies on the working catalyst under operating conditions. The former provides a method of dissecting complex reaction mechanisms into elementary reaction steps and determining their rate constants,[1,2] and the latter provides information on the actual catalytic performance (*i.e.* rates and selectivities under practical reaction conditions). The two techniques were often performed in parallel, probing similar systems, but the continuity between both methods was (and remains) poorly developed. This absence of continuity led to the terms pressure, materials, (and the much less discussed and appreciated) temperature *gaps* between UHV surface science measurements and the reactor studies. Recently we reported the successful multiscaling of the kinetics and mechanism for oxygen-assisted coupling of methanol on gold, obtained from gold

single crystals under ultrahigh vacuum conditions at relatively low temperatures for the prediction of the behaviour of nanoporous gold catalysts over a wide range of predetermined concentrations of adsorbed atomic oxygen under normal catalytic conditions (1 atm, 425 K).[3] Key to this scaling was the use of a transient pressure pulse technique (Temporal Analysis of Products (TAP)[3,4]), which acts as an intermediary between the highly defined surface science studies and the catalytic reactor measurements by analysing the reaction over the actual catalyst at the reactor temperature, while maintaining pressures low enough to ensure Knudsen flow over the catalyst.

The selective oxidative coupling of methanol on gold has been studied and discussed extensively in the previously literature,[5–10] the elementary steps of the catalytic cycle being determined using single crystal studies. Further, nanoporous gold ($Ag_{0.03}Au_{0.97}$, npAu), a bimetallic, well-defined, support free material has been shown to be active, selective, and stable catalyst for the catalytic selective oxidative coupling of methanol.[11,12] Silver is the minority metal in the alloy that facilitates oxygen dissociation, while the host gold alloy drives the catalytic cycle selectively. A key step in the activation of the npAu catalyst for sustained performance under operating conditions is a pre-treatment with ozone[11] which significantly increases the stability and selectivity of the catalyst. It has been shown through use of *in situ* techniques, that the ozone treatment causes an enrichment of the catalyst surface with silver, and produces two types of oxygen species, denoted as *unselective* and *selective.*[13] Under steady state reaction conditions, the unselective oxygen is removed, and the *selective* oxygen species (chemisorbed oxygen atoms) facilitate the high selectivity to methyl formate in the methanol coupling reaction.

In the previously reported work[3] the *selective* oxygen species was isolated for a range of predetermined coverages and its reactivity with methanol probed on the npAu catalyst temperatures near the preferred reactor conditions (425 K) by use of a TAP reactor.[3,4] Using the catalytic cycle and kinetic parameters determined from UHV single crystal studies (refined via the TAP experiments[5]), we predicted trends in the selectivity that showed a smooth transition in product selectivity from low to high pressure and from 200 to 425 K over a range of coverages of selective oxygen.[3] In summary, we demonstrated that the kinetics and mechanism for oxygen-assisted methanol self-coupling determined on single crystal gold in ultrahigh vacuum could be used to predict the reaction selectivity observed over nanoporous gold catalysts under normal catalytic conditions of temperature and pressure. In the work reported here we extend this treatment to predict accurately the selectivities observed in *catalytic flow reactor* experiments across varying temperatures and reactant partial pressures. Further, we rigorously analyse the reaction network, breaking down the kinetic sensitivities for selectivity and rate for each microkinetic step under a range of reaction conditions, graphically illustrating the complex interconnectivities that exist within the network. Under the mild conditions of 1 bar pressure of reactant mixture and 423 K temperature, the selectivity to methyl formate saturates to >99% and becomes insensitive to the rate constants of the individual elementary steps; the selectivity is driven purely by the concentration of the reactants rather than the underlying kinetics. In this regime where the catalyst performance is not *kinetically* limited: it is instead *physically* limited by its active site density.

2. Materials and Methods

2.1 Synthesis and activation of nanoporous gold. The npAu catalyst was synthesised using the previously reported method.[11] 6 karat white gold sheets (15% Au in Ag) were etched chemically with 70% HNO_3 for 30 minutes to remove the Ag, leaving behind approximately 3% Ag in Au.[11,12,14] The remaining HNO_3 is then removed via filtration with water over a quartz frit, and the sample then dried under He flow at 323 K. The npAu catalyst is then activated via temperature ramp from room temperature to 423 K using a concentration of 60 g/Nm^3 of ozone in a 50% O_2/He gas mixture, with a flow rate 50 mL/min at 1 atm and held for a total time of one hour. After ozone treatment the catalyst cooled to 323 K and then is exposed to a stream of 10% methanol and 20% O_2 in He at 1 atm while ramping the temperature to 423 K until constant activity is monitored. The activated catalyst was then transferred to the TAP reactor and evacuated. The structure and morphology of npAu foils resulting from this preparation method were thoroughly studied in previous work.[11] Briefly, the foils are 100 nm thick with 30 to 75 nm ligaments and pore size. As a result of their open and thin structure, mass transfer limitations have been shown to be negligible under all reaction conditions employed in this paper in both the plug flow and TAP experiments.[11]

2.2 Catalytic performance of the nanoporous gold in the flow reactor. The npAu catalyst foils were loaded into a quartz reactor tube (1cm internal diameter), which was then placed in a furnace and the temperature ramped from 323 to 423K under reaction conditions. Typically, the reactant mixture consisted of 10% methanol in 20% O_2 in a He balance at a total flow rate of 50 mL/min, with methanol introduced via a bubbling helium through a methanol flask. To test the effect of temperature on the catalyst selectivity the npAu catalyst was first activated[11] and left under steady state at 423 K until constant activity was recorded (~15 hours), afterwards the sample temperature was dropped to 393 K. The sample was then ramped up with 10 K steps, with a step time of 2.5 hours to allow the sample to reach steady state at each temperature. The effect of reactant partial pressures on catalyst selectivity was also probed. For these experiments the catalyst was first left under steady state at 423 K until constant activity was recorded (~15 hours). The oxygen content of the reaction mixture was fixed at 20% and the methanol content varied from 5% to 20%. Similarly, the test the effect of O_2 concentration, the same process was followed but the methanol concentration was fixed at 10% and the O_2 concentration varied from 5% to 20%.

For all catalytic testing the performances of the npAu catalyst were evaluated by monitoring the exit flow via GC-MS (Column HP-Plot/Q).

2.3 TAP Transient pulse-response experiments The TAP experiments and simulations formed the foundation for the microkinetic modelling; they have been described previously[3] and are only briefly summarized here. The pulse experiments were performed using a commercial TAP-2 type reactor[4] with both pulse and flow capabilities. The pre-activated npAu sample was housed in a *thin zone*[4,15] quartz microreactor, which prior to pulsing was evacuated to $3x10^{-8}$ torr. After activation by flowing a mixture of ozone in oxygen (60 g/Nm^3), the catalyst was exposed to sequential pulses of a methanol/Ar mixture to achieve known initial surface concentrations of selective O. The time-resolved flow of products and unconverted reactant was measured for each methanol pulse at the exit of the microreactor via QMS, and each was quantified (see ref. 3, SI). Argon was included in each reactant pulse to serve as an inert marker.

2.4 TAP Reactor Model. Since a diffusion/reaction analysis of the TAP experiments was used to regress the rate constants obtained from the single crystal studies for use the microkinetic

analysis of the flow reactor, it is briefly described here. The transport model for a thin zone TAP micropulse reactor has been developed extensively.[4,16–19] The transport through the reactor is dominated by Knudsen diffusion, and as such the concentration of any species travelling through the reactor can be defined using the diffusion reaction equation with well-defined boundary and initial conditions

$$\frac{dC_i}{dt} = \frac{D_i}{\varepsilon_b}\frac{d^2C_i}{dz^2} \pm R \tag{1}$$

C is the concentration of the gaseous species i (mols/cm^3), D is the Knudsen diffusivity of the gas i (cm^2/s), ε_b is the fractional voidage of the reactor, z denotes the reactor coordinate, t is the time (s), and R is the rate equation for species described by C. Indeed, as determined by rare gas pulses, the reactor is well mixed by Knudsen diffusion as configured.[3,4] To precisely describe the time response of the effluent flux of species from the TAP reactor, the equation was modelled via the technique described previously[5] using the MATLAB (R2016b) programming environment[20] and a 4th order Runge-Kutta algorithm as implemented in the ODE15s solver in MATLAB.[21] The physical parameters utilized in the TAP reactor model are the same as previously published.[5]

The validity of the transport model, which governs the effluent flux of all species from the reactor, was verified by the fact that the measured transient response observed following an argon pulse into the reactor agreed precisely with the transport analysis (Eqn. 1, R = 0). For an inlet condition of a pulse of 10^{15} molecules of Argon, the *mean pressure*[5] recorded in the centre of the catalyst zone is computed to be ~10^{-5} bar (10 millitorr) at 423 K.

2.5 Plug Flow Reactor Analysis The reactor was described as isothermal and one dimensional plug flow using a the equation.[22]

$$\frac{dC_i}{dt} = -\upsilon\,\frac{dC_i}{dV} + R \tag{2}$$

Where C_i is the concentration of the gas species i (molecules/cm^3), υ is the volumetric flow rate (cm^3/s) V is the volume of the reactor (cm^3) and, similar to Eqn. (1) from the TAP analysis, R is the mean field kinetic expression used to describe the rate of formation of species i in the reaction network (see below). To evolve the system along the axial coordinate of the reactor dV was taken as AdL where A s the cross-sectional area (cm^2) of the reactor, and dL is a step in length along the reactor (cm). While for linear kinetic sequences it is possible to solve the rate equations at steady state, for the network used in this work, which contains multiple nonlinear branching steps, it is more efficient to simply evolve the system temporally using Eqn. (5). In this work the reactor was broken down into a grid of 10 plugs of uniform volume, (with $V = \sum dV$) then using the initial condition of zero reactant partial pressure in the reactor, and a constant inlet of reactant gas it is possible to temporally evolve the system. The first initial condition (at $t = 0$) is expressed using:

$$C_{n=1} = C_{inlet} \tag{3}$$

Where n is the integer representing a grid point. At the inlet of the reactor (the first grid point, $C_{n=1}$) the concentration is set to that of the reactant gas mixture (C_{inlet}) and is held constant. Initially,

$$C_n = 0\ ,\ \mathrm{L} > 0. \tag{4}$$

5

To allow the system to evolve spatially, the method of lines is used.

$$\frac{dC_{n,j+1}}{dt} = -\upsilon \frac{(C_{n,j} - C_{n-1,j})}{(V_n - V_{n-1})} - R_n \tag{5}$$

with n being the integer representing the grid location (n > 1, as at n = 1 there is a constant inlet concentration of reactant gas); j represents the concentration recorded at a time j. Similar to the TAP analysis, the system was evolved temporally using the 4th order Runge-Kutta algorithm as implemented in the ODE15s solver in MATLAB.[21] To determine product concentrations the reactor was allowed to reach steady state, which, depending on reactant conditions, took from 3 to 30 minutes. For the plug flow reactor simulations in this work, the volumetric flow rate was set to 50 cm^3/min, with reactor dimensions of 1 cm in length and 1.0 cm in diameter, and the catalyst loading was set to 17 mg to match experiment, with a catalyst surface area of 2.0 m^2/g. As all concentrations are recorded in molecules/cm^3 (gaseous) and molecules/cm^2 (surface bound) a scaling of catalyst surface area per reactor volume in a plug is required, which we have denoted Q, and has the dimensions (cm^{-1}).

$$Q = \frac{S_{cat}}{V_{reactor}} \tag{6}$$

With S_{cat} being the catalyst surface area (cm^2), and $V_{reactor}$ (cm^3) being the reactor volume. Therefore, when calculating the rate of adsorption/reaction of a gaseous species with a surface concentration equation (5) is expanded to include the surface area to volume scaling.

$$\frac{dC_{n,j+1}}{dt} = -\upsilon \frac{(C_{n,j} - C_{n-1,j})}{(V_n - V_{n-1})} - R_n Q \tag{7}$$

A typical temporal and spatial product evolution for the standard experiment (0.1 bar methanol, 0.2 bar oxygen, 423 K) are shown below (Figure 1).

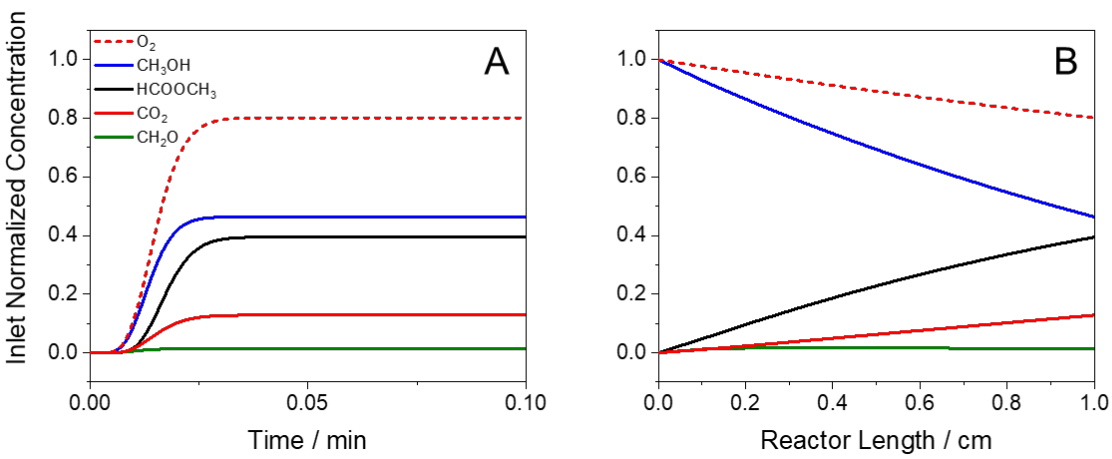

Figure 1. A) The temporal evolution of gaseous products at the reactor exit normalised to the inlet reactant concentrations. B) Spatial evolution of gaseous products under steady state normalized to the inlet reactant concentrations. Reaction conditions were set at 0.1 bar methanol, 0.2 bar oxygen, and 423 K.

2.6 The Microkinetic Model. The rate expression, Ri, for each species involved in the network for oxidative self-coupling of methanol over npAu[4,5] (Figure 2) is given by Eqns. (8) – (20).

$$r[CH_3OH] = k_{1a}[CH_3OH][O^*] \tag{8}$$

$$r[CH_2O] = +k_{3a}[CH_2O^*] - k_{3b}[CH_2O] \quad (9)$$
$$r[HCOOCH_3] = +k_9[HCOOCH_3^*] \quad (10)$$
$$r[CO_2] = +k_6[HCO_2^*] \quad (11)$$
$$r[CH_3O^*] = +k_1[CH_3OH][O^*] - (k_7[CH_2O^*] + k_2)[CH_3O^*] \quad (12)$$
$$r[CH_2O^*] = +k_2[CH_3O^*] + k_{3b}[CH_2O] - (k_{3a} + k_7[CH_3O^*] + k_{4a}[O^*])[CH_2O^*] + k_{4b}[H_2CO_2^*] \quad (13)$$
$$r[H_2COOCH_3^*] = +k_7[CH_3O^*][CH_2O^*]-k_8[H_2COOCH_3^*] \quad (14)$$
$$r[HCOOCH_3^*] = +k_8[H_2COOCO_3^*]-k_9[HCOOCH_3^*] \quad (15)$$
$$r[H_2CO_2^*] = +k_{4a}[CH_2O^*][O^*]-k_{4b}[H_2CO_2^*]-k_5[H_2CO_2^*] \quad (16)$$
$$r[HCO_2^*] = +k_5[H_2CO_2^*] - k_6[HCO_2^*] \quad (17)$$
$$r[O_2] = -k_{Oa}[O_2](1 - \theta) + k_{Ob}[O^*] \quad (18)$$
$$r[O^*] = +k_{Oa}[O_2](1 - \theta) - k_1[CH_3OH][O^*]/2 - k_2[CH_3O^*]/2 - k_{4a}[CH_2O^*][O^*] + k_{4b}[H_2CO^*] - k_5[H_2CO_2^*]/2 - k_6[HCO_2^*]/2 - k_8[H_2COOCH_3]/2 - 2kO_b[O^*] \quad (19)$$
$$\theta = ([O^*] + [HCO_2^*]) / (\theta_{density}\ \theta_{sat}) \quad (20)$$

The reaction network consists of 13 kinetic steps, of which four (k_6, k_8, k_9, and k_{Ob}) were determined to have no significant effect on selectivity (see below). Thus, 9 rate constants are determined to be selectivity-defining, meaning changes in their values significantly effect selectivity (Table 1).

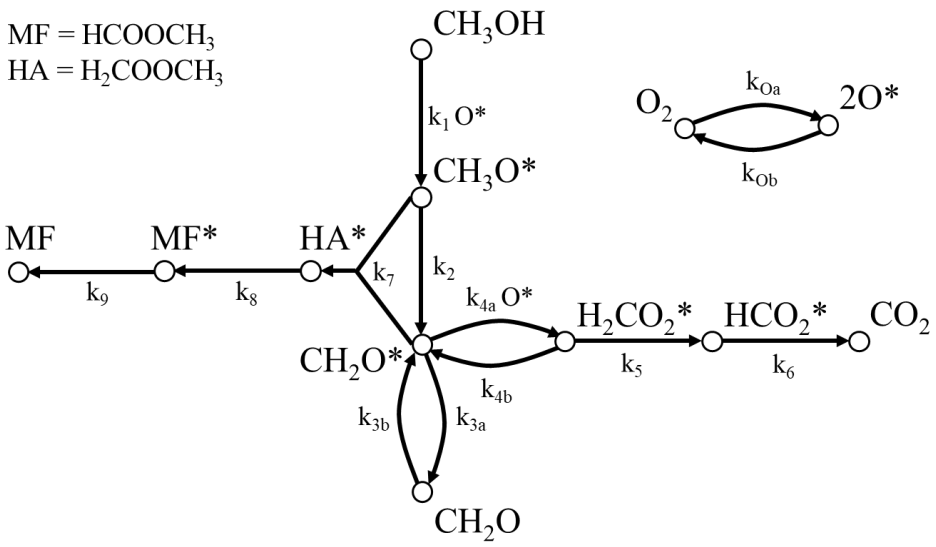

Figure 2. Network used for simulation and analysis of methanol oxidation over O* treated npAu. Nodes indicate species, with edges representing rates of transformation. Pathways that do not contribute to the selectivity of the oxidized products (*e.g.* formation of H* / OH* / H_2O*) are not modelled explicitly.

The inclusion of the rate of activation of dioxygen and site blocking by adsorbed species in steady-state conditions are essential for quantitative comparison of predictions from UHV and TAP based kinetic information to the flow reactor experiments. For the plug flow simulation, as oxygen is co-fed into the reactor with methanol, the formation and consumption of the selective oxygen species was accounted for by including O_2 dissociation (k_{Oa}) and recombination of atomic oxygen (k_{Ob}) (Eqns. (18) to (20), Figure 2) and the rate of O* consumption by reaction with other species (Figure 2, steps k_1, k_{4a}, and k_{4b}), both having been determined previously.[5,23] Since H_2 was not detected in the plug flow experiments, it was

assumed all H* formed rapidly reacts to make water, consuming O*. To accurately calculate the effect of each step involving non-oxidative C-H cleavage (k_2, k_5, k_6, k_8, and k_9) on the rate of O* consumption (giving rise to the formation of hydroxyls and subsequentially water), we assumed instantaneous reaction of the H* released with adsorbed O* to form water (Eqn. 19). It has been demonstrated previously that the oxygen coverage saturates at approximately 10^{-2} monolayers, the density of active sites for O_2 dissociation.[23,24] We assume that both oxygen and formate compete for active sites. This effect is included specifically in Eqn. (21), where $\theta_{denisity}$ is the atomic density of gold (in cm^{-2}), and θ_{sat} represents the saturation coverage of active sites in fractional monolayers (0.01 ML).

Table 1. Kinetic parameters for the oxidative self-coupling of methanol reaction network shown graphically in Figure 2 and explicitly in Eqns. (8) – (20). Steps that are shaded do not affect the catalytic selectivity any measurable amount.

Step	Pre-Exponent	Units	Ea / kJmol^{-1}	References
k_1	4.61×10^{-14}	cm^3/s	17.00	23
k_2	1.23×10^{15}	s^{-1}	67.83	5
k_{3a}	3.03×10^{16}	s^{-1}	40.74	5
k_{3b}	0.25†	-	-	5
k_{4a}	1.95×10^{-2}	cm^2/s	34.60	5
k_{4b}	1.44×10^{14}	s^{-1}	38.89	5
k_5	4.45×10^{13}	s^{-1}	52.46	5
k_6	5.79×10^{14}	s^{-1}	95.82	5,25,26
k_7	3.11×10^{-2}	cm^2/s	19.56	5
k_8	5.79×10^{14}	s^{-1}	31.96	5,6
k_9	1.49×10^{16}	s^{-1}	55.60	5,26
k_{Oa}	3.69×10^{-1}	s^{-1}	20.92	24
k_{Ob}	7.63×10^{14}	s^{-1}	156.39	5,8,26

† Indicates sticking probability.

2.7 Data analysis and model regression. All reactor modelling and data analysis was performed using the MATLAB (R2016b)[20] programming environment, using in-house purpose-built scripts.

3. Results

3.1 Using the mechanism determined in ultrahigh vacuum experiments and the associated rate constants to predict selectivity under catalytic flow reactor conditions

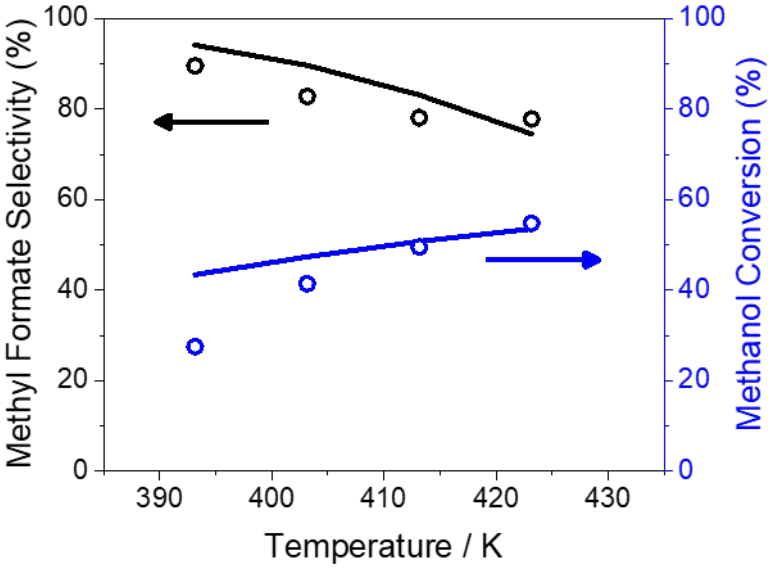

Figure 3. Conversion and selectivity from methanol coupling reaction using 10% methanol in 20% oxygen at temperatures varying from 393 to 423 K. Solid lines represent plug flow analysis; circles represent catalytic flow reactor data. Under all conditions probed, CO_2 was the only other product detected.

The effect of temperature on the methanol conversion and the selectivity to methyl formate over the npAu catalyst was measured in the flow reactor at temperatures ranging from 393 to 423 K (open circles, Figure 3). Under standard plug flow conditions (section 2.2) as the temperature was decreased from 423 to 393 K, the methanol conversion dropped from 55 to 25%. Inversely, the selectivity to methyl formate increased, approaching saturation at 100% as the temperature was decreased. The plug flow analysis recreated the experimentally measured methyl formate selectivity well within experimental uncertainties at the conditions of the catalytic flow reactor (0.1 bar methanol, 0.2 bar oxygen partial pressure) using the rate constants in Table 1 (solid lines, Figure 3). *It is important to emphasize that this prediction of the catalytic selectivity in the plug flow reactor is obtained from kinetics and mechanism determined on single crystal gold surfaces using ultrahigh vacuum methods*. We attribute the small differences between the predicted and measured conversion at 393 K to the slow decomposition of surface-bound formate, which causes blockage of the active sites for O_2 dissociation, thereby lowering availability of selective oxygen and consequently the methanol conversion. For example, under these conditions approximately 50% of the active sites are computed to be occupied, of which 10% of the sites are formate and 38% are oxygen. As the decomposition of formate was estimated using TPRS desorption peak temperatures[5] rather than explicitly regressed using the TAP model, the differences in conversion can be considered within the error of the estimation technique.

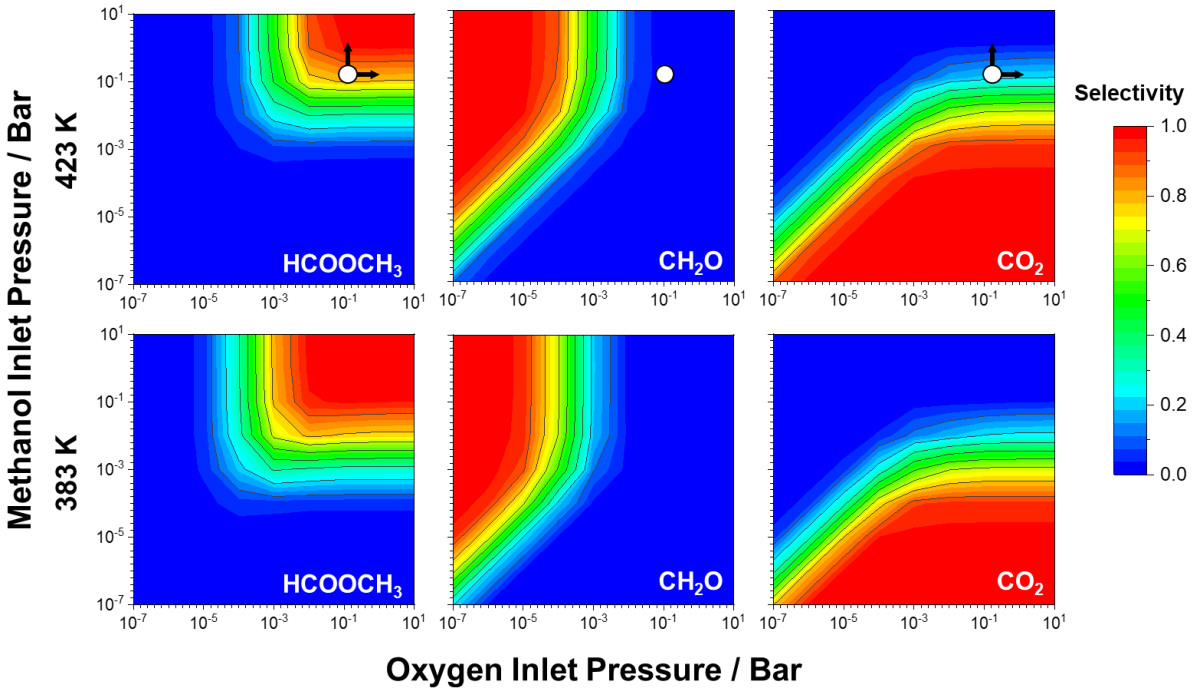

Figure 4. Plug flow reactor simulation with methanol and oxygen co-fed in at partial pressures varying from 10^{-7} to 10^{1} bar at 423 and 383 K. Circles represent conditions used in catalytic flow reactor (10% methanol, and 20% O_2 in a He balance at 1atm), with the attached arrows indicating experimentally measured selectivity trends (Figure S2). In both cases methyl formate selectivity increases with increasing methanol pressure.

In order to predict the effect of reactant partial pressures on the reaction selectivity, the plug flow analysis was extended to inlet reactant pressures from 10^{-7} to 10^{1} bar, and the selectivities computed at different temperatures (Figure 4). The contour plots for selectivity predict clear effects of increasing either the methanol or oxygen partial pressures from the standard operating conditions. We thus performed further steady state experiments at constant temperature in the flow reactor, changing either the methanol or oxygen partial pressures from the standard operating condition to test the predictions of the analysis (see arrows, Figures 4 and S2). Indeed, increasing the methanol partial pressure increased selectivity to methyl formate, and changing the oxygen partial pressure had less effect, as predicted. At all oxygen pressures it was found that as the pressure of methanol is increased the selectivity to methyl formate increases, consistent with the trend observed with increasing O coverage seen in the previous TAP reactor simulations.[5]

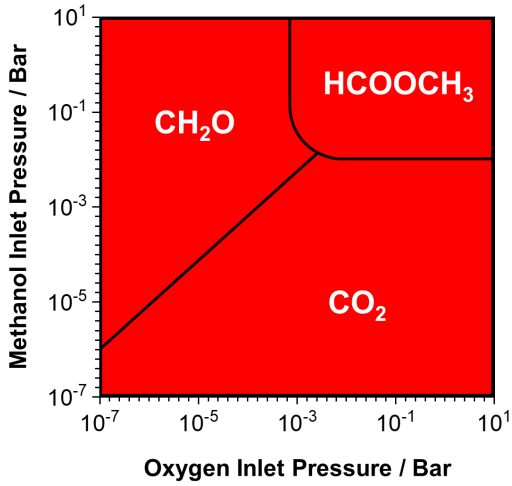

Figure 5. Selectivity phase diagram for the methanol self-coupling reaction at 383 K indicating the regions where either formaldehyde, methyl formate, or CO_2 is the major product (> 50% selectivity).

The contour plots (Figure 4) clearly show distinct regions of selectivity for each of the three products (Figure 5). First, when the reactant pressures are both above 10^{-2} bar, methyl formate is the dominant product. Second, when the methanol is in excess and the oxygen pressure below 10^{-3} bar, formaldehyde becomes the dominant product. Finally, if oxygen is in excess and the methanol pressure below 10^{-2} bar, CO_2 is the dominant product. At all oxygen pressures it was found that as the pressure of methanol is increased the selectivity to methyl formate increases. Furthermore, the reactor analysis allows prediction of the selectivity changes that would accompany changes in temperature in the reactor across a variety of reactant partial pressures (Figure 4). Decreasing the operating temperature increases the size of regime where methyl formate is dominant (Figure 4), increasing the selectivity to methyl formate under lower reactant pressure conditions, at the cost of decreasing conversion per gram of catalyst (see Figure 3).

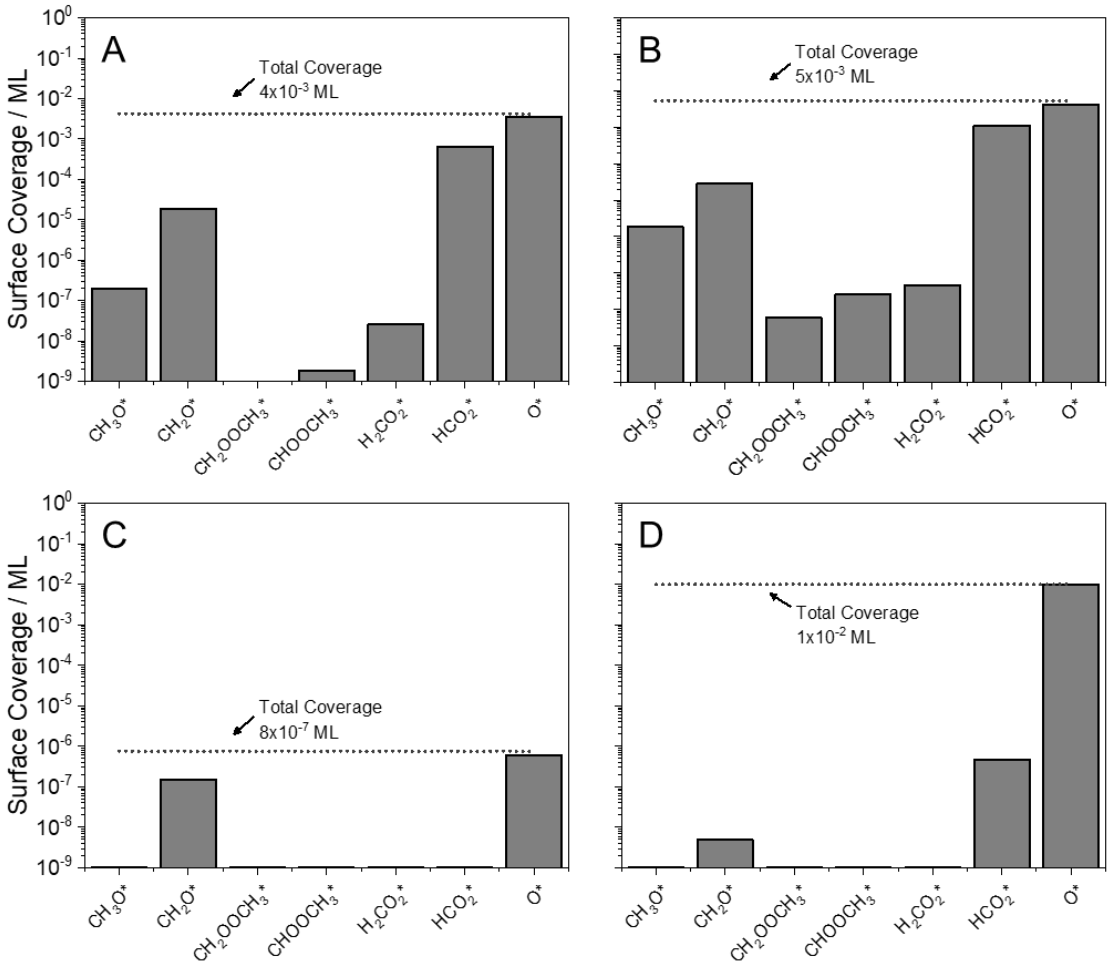

Figure 6. Surface coverages of species computed from the plug flow model at 423 K. A) Inlet methanol partial pressure of 10^{-1} bar and a 1:2 methanol to oxygen ratio, 77% selectivity to methyl formate, 23% selectivity to CO_2 was observed, with a total site density of $4x10^{-3}$ ML. B) Inlet methanol partial pressure of 1 bar and a 1:2 methanol to oxygen ratio, >99% selectivity to methyl formate with a total site density of $5x10^{-3}$ ML. C) Inlet methanol partial pressure of 10^{-1} bar and 5000:1 methanol to oxygen ratio, >99% selectivity to formaldehyde with a total site density of $7x10^{-7}$ ML. D) Inlet oxygen partial pressure of 10^{-1} bar at 1:5000 methanol to oxygen ratio, >99% selectivity to CO_2 with a total site density of $1x10^{-2}$ ML, saturating all active sites.

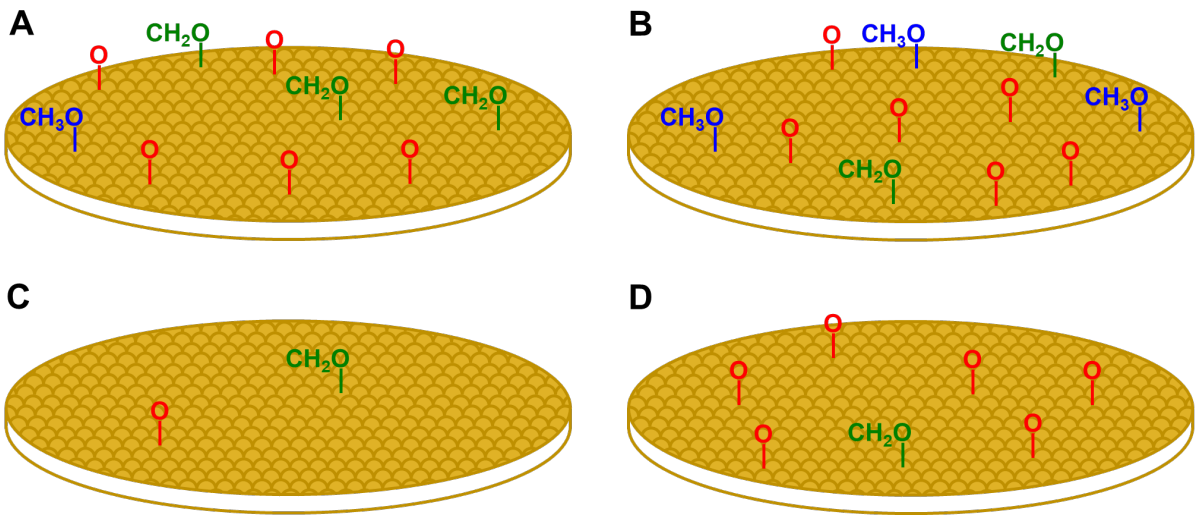

Figure 7. Schematic representation of the relative concentration of intermediates on the catalyst surface under different reaction conditions A) Inlet methanol partial pressure of 10^{-1} bar and a 1:2 methanol to oxygen ratio. Due to the higher concentration of adsorbed formaldehyde, combustion is more prominent than coupling. B) Inlet methanol partial pressure of 1 bar and a 1:2 methanol to oxygen ratio. Due to the increased balance of methoxy and adsorbed formaldehyde, coupling dominates. Formaldehyde and O populate the surface sparsely so that combustion is the dominate route. C) Inlet methanol partial pressure of 10^{-1} bar and 5000:1 methanol to oxygen ratio. The high methanol to oxygen ratio produces >99% selectivity to formaldehyde. D) Inlet oxygen partial pressure of 10^{-1} bar at 1:5000 methanol to oxygen ratio. The high excess of oxygen produces >99% selectivity to CO_2. CH_2COOCH_3*, $CHOOCH_3$*, H_2CO_2* and HCO_2* are not displayed for clarity.

The surface concentration of the adsorbed intermediates under different reaction conditions, computed from the plug flow analysis, yields deeper insight into the surface reactions. Under the standard conditions employed in the flow reactor studies, which favour methyl formate, the surface oxygen coverage is ~4×10^{-3} ML (Figures 6A, 7A), which is close to previous estimates of the surface site density for O_2 dissociation.[24] Perhaps surprisingly, the most abundant reaction intermediate (outside of adsorbed O*) is the adsorbed formate, the predecessor to CO_2 formation, with the concentrations of adsorbed methoxy and formaldehyde, the precursors to methyl formate formation, being much lower. The lesser production of CO_2 under these conditions is accounted for by the relatively slow rate of decomposition of formate, not its surface concentration.

Increasing the pressure of the reactants to 1 bar increases the selectivity for methyl formate to >95 %, due to a 100-fold increase in the surface concentrations of methoxy and a 10-fold increase in formaldehyde (Figures 6B, 7B), which are the precursors to methyl formate production. As the reactant pressures are increased to beyond 1 bar the selectivity saturates at >99% methyl formate. Under methanol rich conditions and oxygen partial pressures less than 10^{-3} bar, the total surface coverage is very low (8×10^{-7} ML), and only formaldehyde is expected to form (red region, Figure 4, Figure 5). Under these conditions the dominant surface intermediate is adsorbed formaldehyde (Figures 6C, 7C). Excess methanol keeps the surface coverage of oxygen very low by reacting away the selective O* to form methoxy. Since the rate of C-H cleavage of methoxy to yield formaldehyde is not dependent on oxygen coverage,

this greatly increases the fractional coverage of formaldehyde relative to other surface intermediates. Therefore, the probability of a formaldehyde molecule re-adsorbing and finding a reactive intermediate (O* or CH_3O*) is very low, facilitating the dominance of formaldehyde. Conversely, under methanol lean conditions and oxygen partial pressures exceeding 10^{-3} bar, CO_2 is the dominant product (red region, Figure 4, Figure 5). When the relative partial pressure of oxygen is relatively high, the reaction with methanol with adsorbed O is slower than the rate of oxygen dissociation, and adsorbed O dominates the intermediates on the surface (Figures 6D, 7D). Therefore, when formaldehyde is formed from C-H cleavage of methoxy, its probability of reacting with chemisorbed oxygen to form adsorbed formate and, subsequently CO_2, is high (Eqns. (14) and (17)). Under all conditions the total surface coverage by intermediates is sufficiently low that it is unnecessary to consider lateral interactions.

3.2 Selectivity–controlling intermediates In the previous TAP analysis the fractional coverage of methoxy at all reaction temperatures and all fixed O coverages was shown to correlate well with the selectivity to methyl formate.[5] Under plug flow conditions, however, where the oxygen coverage is dependent on reactant partial pressures, this relationship becomes less predictive. A better, more consistent correlation under steady flow conditions is obtained with the steady state coverage of methoxy (Figure 8A) across all methanol and oxygen partial pressures. This relationship also extends to the TAP pulse simulations if the mean methoxy coverage (denoted as the half height of the transient pulse) is utilised (Figure 8B). Thus, a strong positive correlation is found between steady state surface coverage of methoxy and methyl formate selectivity, *independent of inlet reactant pressures*, demonstrating that the methoxy coverage is the predominant factor defining methyl formate selectivity. Fractional selectivities to methyl formate approach 1.0 at mean methoxy coverages well below the active site density.

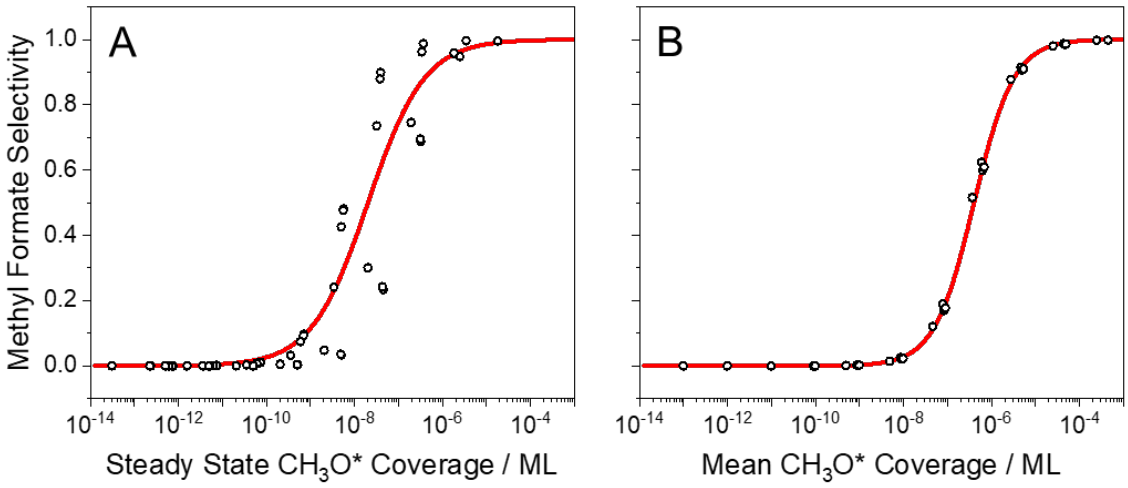

Figure 8. A) Steady state methoxy coverage vs selectivity to methyl formate from plug flow co-feed simulation, with oxygen and methanol pressures varied from 10^{-5} to 10^{-1} bar, at 423 K. B) Mean methoxy coverage recorded during TAP pulses vs selectivity to methyl formate taken from TAP simulation with mean methanol pressure varying between 10^{-7} and 10^{1} bar, with fixed oxygen coverages of 10^{-1} to 10^{-7} monolayers at 423 K. Solid red lines represent the best fit.

3.3 *Degrees* of Selectivity and Rate Control of Elementary Steps Certain elementary steps in the catalytic cycle may have more effect on the selectivity (and overall rate) than others. The degree of selectivity control (DOSC) and the degree of rate control (DORC)[27,28] were determined from the plug flow simulation across a wide range of partial pressures of oxygen and methanol. This sensitivity analysis assesses the degree of dependence of the selectivity/rate on individual elementary steps in the reaction mechanism. A DOSC equal to unity means that the step is selectivity enhancing (an increase in the rate constant will increase overall selectivity for a given product), and a DOSC of minus one means that the step is selectivity inhibiting (an increase in the rate constant will decrease selectivity). Values between these limits indicate a proportional amount of selectivity promotion or inhibition, with a DOSC of 0 showing the step has no effect on selectivity.

The DOSC was calculated using

$$DOSC_{k_j} = \frac{d \ln (X_i)}{d \ln (k_j)} \tag{21}$$

DOSC is the degree of control for the jth elementary step, k_j is the rate constant for that step, and X_i is the selectivity to a given product i. For the analysis all rate constants except k_j were fixed. The DOSC for each product was computed at 423 K for a range of methanol and oxygen inlet partial pressures for all of the microkinetic steps shown in Figure 2 (see supporting information). The DOSC is shown only for microkinetic steps k_1, k_2, k_{3a}, k_{4a}, k_7, and k_{Oa}. For the steps k_{3b}, k_{4b}, and k_5, it was found that $DOSC_{k_{3a}} = -DOSC_{k_{3b}}$ and that $DOSC_{k_{4a}} = -DOSC_{k_{4b}} = DOSC_{k_5}$ under all conditions probed. The steps (k_6, k_8, k_9, and k_{Ob}) were found to have zero (or near zero) degree of selectivity control under all conditions probed.

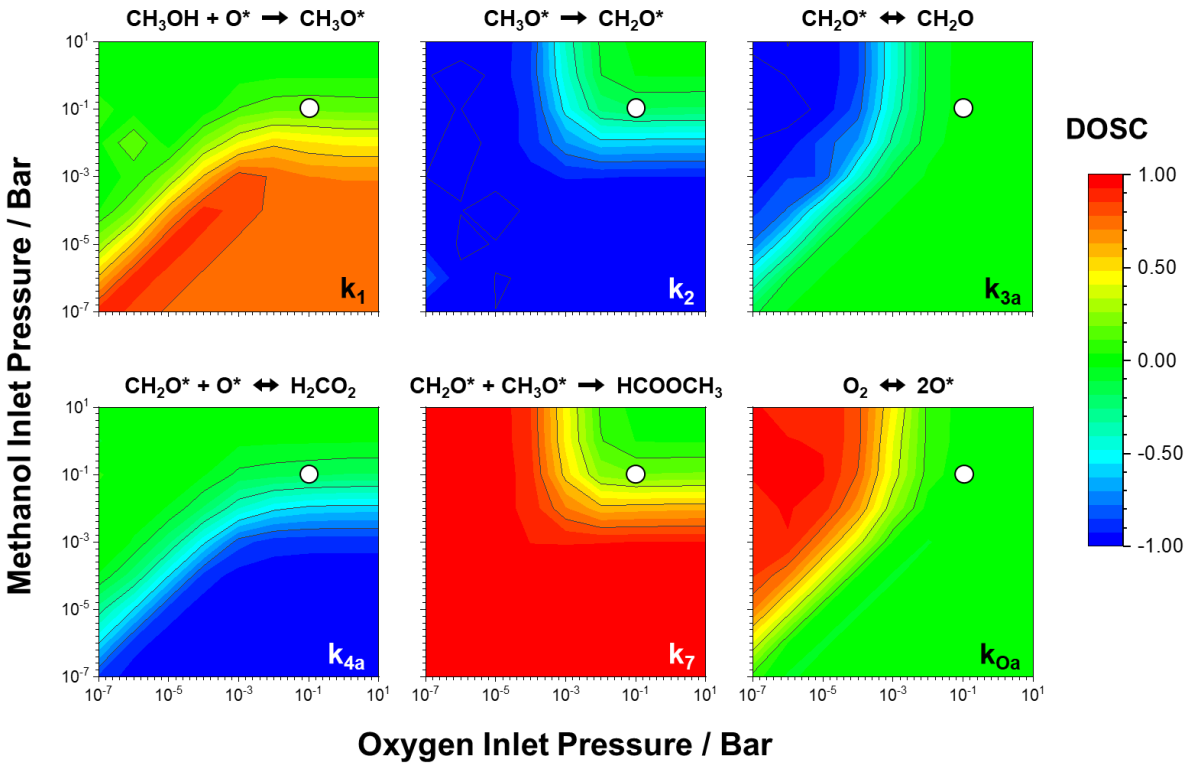

Figure 9. Degree of selectivity control (DOSC) for methyl formate formation for the six selectivity-defining elementary steps computed from the plug flow reactor simulation with oxygen and methanol partial pressures varying between 10^{-7} to 10^{1} bar at 423 K. When both reactant pressures exceed one bar, the degree of selectivity control falls to zero for each step. Circles represent conditions used in catalytic flow reactor.

Perhaps the most significant result of this degree of selectivity analysis is the prediction of *kinetic saturation of selectivity* in all three regimes of reactant pressures where a single product dominates (Figures 4, 5). For example, when the partial pressure of both reactants exceeds about 0.1 bar, the DOSC for methyl formate production for all the elementary steps falls to zero, indicating insensitivity to changes in the rate constants (Figure 9). The selectivity approaches ~100% methyl formate under these conditions (Figure 4). This result indicates that under certain conditions, for a given mechanistic network, the selectivity to a given product can *saturate*; the selectivity is driven solely by the concentrations of reactants. Therefore, under certain conditions of pressure and temperature, very significant changes in the rate constants are required to change the selectivity appreciably, essentially buffering the selectivity from changes in temperature. Similar behaviour is predicted for formaldehyde (Figure 10) and CO_2 production (Figure S3).

In the case of oxygen-assisted self-coupling studied here the *selectivity saturation* is a consequence of the network itself (Figure 2). If the concentration of the primary self-coupling intermediate (in this case methoxy) is high enough that the rate of coupling (k_7) is significantly larger than the rate of combustion (represented by k_{4a}) or desorption (represented by k_{3a}), the selectivity becomes insensitive to modest changes in the kinetic parameters. For this self-coupling network, the rate of methoxy formation can be increased by increasing both the methanol and oxygen concentration (Eqn. (8)) as was demonstrated by the experiments in the flow reactor (arrows, Figure 4). Therefore, *independent* of the values for the rate constants, as the pressure of both reactants are increased, the network will always favour self-coupling. Due to the similarity in their reaction networks[7,29], this high-pressure *saturation* would be expected for all alcohol self-coupling reactions.

Outside the regions of selectivity saturation interesting trends in the DOSC emerge. As expected from the above discussion, steps that tend to increase the surface concentration of methoxy and formaldehyde show a high positive degree of selectivity to methyl formate, and the steps that tend to decrease their concentration show the opposite strongly negative value. Thus, increasing the rate of formation of methoxy from the reaction of methanol and O* (k_1) leads to a higher methoxy concentration and higher selectivity to methyl formate, whereas increasing the rates of methoxy decomposition (k_2) and/or consumption of formaldehyde by reaction with adsorbed O (k_{4a}) or shifting the adsorption equilibrium for formaldehyde (k_{3a}) tend to decrease the selectivity for methyl formate. The rate of O_2 dissociation per unit area also positively effects selectivity by increasing the concentration of O*, which subsequently increases the rate of methoxy formation.

There are significant non-obvious interrelationships among the steps in the reaction network (Figure 9); in some cases, the sum of the DOSC of two steps is equal to zero across all conditions probed. For example, as may seem counterintuitive, increasing the rate constants

for both methoxy dehydrogenation (k_2) and the reaction of methoxy with formaldehyde (k_7) results in no change in selectivity (Figure 9, centre panels). The origin of this counterbalancing of kinetic steps is apparently the strong relationship between the concentration of adsorbed methoxy and the selectivity (Figure 8). Increasing the rate constants for both the bimolecular reaction (k_7) and the rate of methoxy dehydrogenation ensures that the increased amount of formaldehyde formed by dehydrogenation will favourably react with methoxy. Other elementary steps mirror one another with respect to their degree of selectivity control in different regions of catalytic selectivity (Figure 5). O_2 dissociation (k_{Oa}) and formaldehyde desorption (k_{3a}) are enhancing or inhibiting, respectively, in cases that favour formaldehyde production (Figures 4, 5, and 9). At the boundaries of these regions of complementarity the selectivity to methyl formate depends markedly on reactant concentrations.

The result of this complementarity is that certain kinetic steps are linked, as is evident by visual inspection of Figures 9 and 10. For example, the domain where k_7 enhances methyl formate selectivity, k_2 is inhibiting, and when combined they have a net DOSC ≈ 0. Any shift in the value of k_7 can be compensated by the same shift in k_2. Similar interrelationships are seen for k_1 and k_{4a} and for k_{3a} and k_{Oa}. The DOSC contours for CO_2 demonstrate very similar qualities to the DOSC for methyl formate (see Figure 9 and S3), with the same kinetic steps being complementary. However, the DOSC for steps k_1 and k_7 is subtracted by 1 and the DOSC for steps k_{4a} and k_2 is increased by 1, with the DOSC for steps k_{3a} and k_{Oa} staying same. The DOSC contours for formaldehyde (Figure 10) demonstrate that, differing from methyl formate and CO_2, only steps k_2 and k_7 are considered complimentary. The origin of these relationships and their implementation in practice requires further study, but the analysis demonstrates potentially useful complex relationships between catalytic selectivity and the kinetics of the elementary steps.

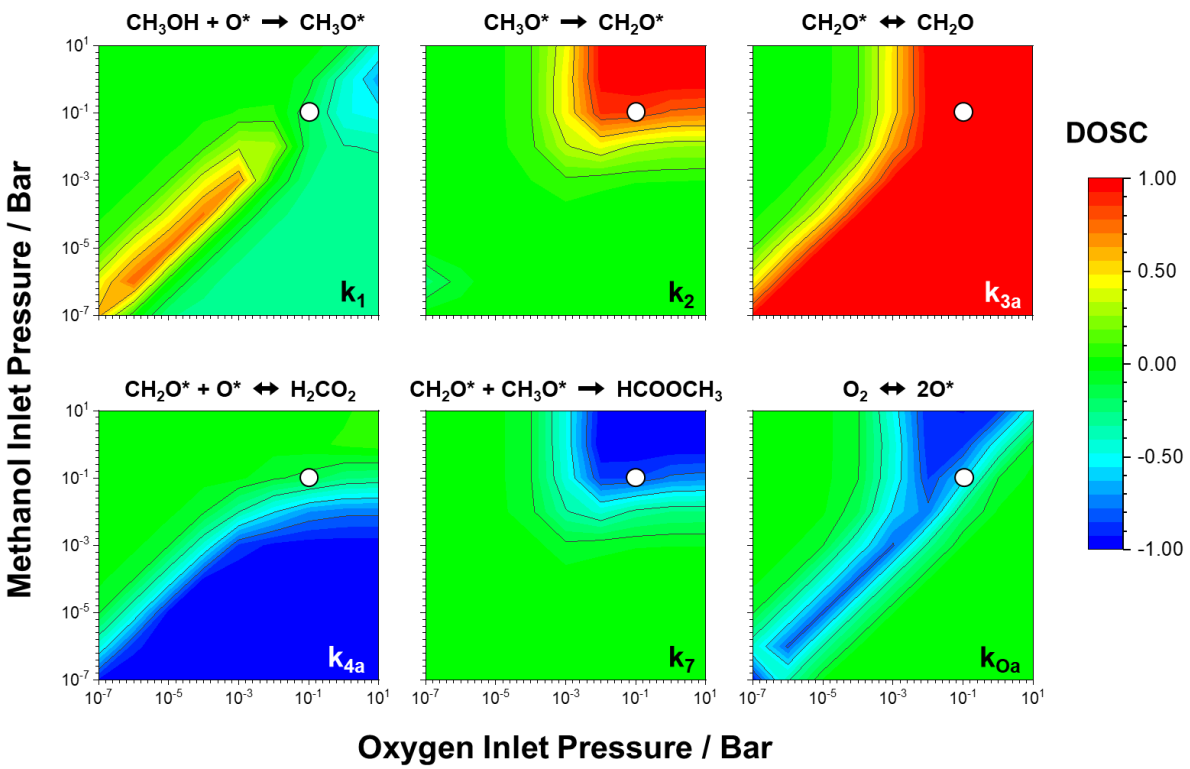

Figure 10. Degree of selectivity control (DOSC) for formaldehyde formation for the six selectivity-defining elementary steps computed from the plug flow reactor simulation with oxygen and methanol partial pressures varying between 10^{-7} to 10^{1} bar at 423 K. When the methanol to oxygen ratio is >> 1 and the oxygen pressure is < 10^{-2} the degree of selectivity control for all steps falls to zero. Circles represent conditions used in catalytic flow reactor.

3.4 Degree of and Rate Control The degree of rate control (DORC) and degree of selectivity control (DOSC) for all three products show the same trends (Figures 9-11, S3-S5), albeit with slight shifts in the domains, over the range of partial pressure values. Under reactant partial pressures approaching 1 bar, where the DOSC for methyl formate for each kinetic step saturates at zero, the DORC for steps k_2, k_{3a}, k_{4a}, k_7 also saturated to zero. However, for steps k_1 and k_{Oa} it *did not* (Figure 11), demonstrating that while the selectivity to methyl formate may become independent of changes in the rate constants in this pressure regime, the *rate of production* of methyl formate does not. The general implication of this feature is that for certain reaction networks operating conditions may exist under which selectivity and conversion become only weakly interrelated.

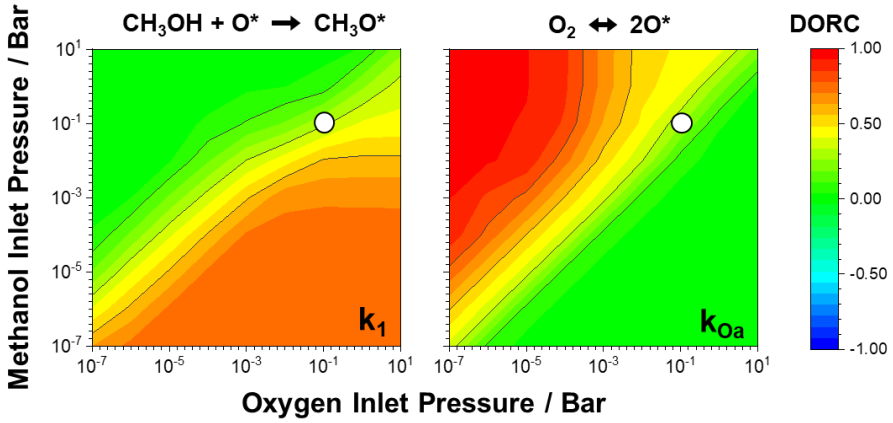

Figure 11. Degree of rate control (DORC) for methyl formate formation for steps k_1 and K_O computed from the plug flow reactor simulation with oxygen and methanol partial pressures varying from 10^{-7} to 10^{1} bar at 423 K. Differing from the DOSC, the DORC maintain significant positive values at partial pressures used in the reactor. Circles represent the conditions used in the catalytic flow reactor.

3.5 Catalysis by Design

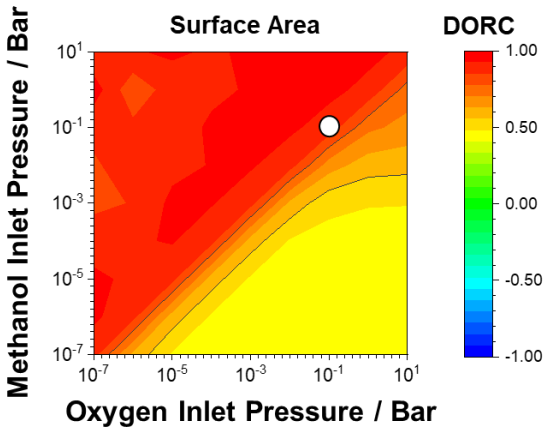

Figure 12. Degree of rate control (DORC) for methyl formate formation for the catalyst surface area computed from the plug flow reactor simulation with oxygen and methanol partial pressures varying from 10^{-7} to 10^{1} bar at 423 K. The surface area is rate limiting under all conditions probed, at the standard reaction conditions (denoted by the open circle) the DORC for the surface area is 0.9.

The "holy grail" of catalysis is *catalysis by design*, the capability of accurately predicting catalytic behaviour and designing catalytic systems with optimum selectivity and production rate with a minimum of experimental data. Through rigorous kinetic analysis, based on understanding of the kinetics and mechanism from studies of surface reactivity in ultrahigh vacuum on single crystals and Knudsen flow conditions on the actual catalyst, we have predicted the catalytic selectivity for a complex reaction network under realistic catalytic flow conditions. Analysis of the reaction demonstrates that the oxidative self-coupling of methanol over nanoporous gold can be driven to nearly 100% selectivity to methyl formate under the relatively mild conditions near 1 bar of reactants and temperatures of 385 - 423 K, with little sensitivity to minor changes in the rate of all microkinetic steps (Figure 9). It has also been shown that the production rate *under these limiting conditions* only depends significantly on the rate of reaction of methanol with O* and the dissociation rate of O_2, both of which can increased by increasing the density of sites active for O_2 dissociation (Figure 11). To further demonstrate the effect of increasing the active site density, the DORC was calculated according to Eqn. (21), but with Q being the variable (see Eqns. 6,7) instead of a given rate constant (k_j). Under all conditions probed changing the surface area is rate limiting (Figure 12) even under the conditions which lead to saturation in the selectivity (Figures 9-11 S3-S6). Thus, under these conditions an increase in surface area is the most effective way to increase catalytic activity.

Conclusions

Plug flow microkinetic analysis of the oxidative self-coupling of methanol using the catalytic cycle and elementary step kinetics obtained from single crystal studies, the latter fine-tuned using product pulse responses obtained in a TAP reactor, predicts well the selectivities and conversion observed in a catalytic flow reactor with varying temperature and reactant partial pressures. The analysis shows that methyl formate selectivity is enhanced by increasing the concentration of surface bound methoxy, by appropriate choice of reactant partial pressures. From the analysis a phenomenon of *kinetic saturation* of *selectivity* was discovered; the overall selectivity to a methyl formate becomes insensitive to the rate constants of the elementary steps.

Utilising the degree of selectivity and rate control, complex relationships between kinetic steps and product selectivity were elucidated, indicating that the selectivity (and rate) enhancing steps are highly dependent on the reactant conditions, and that the effects of certain elementary steps on selectivity are strongly correlated with one another. This extensive kinetic study affords in-depth knowledge of the catalytic system, connecting performance across a wide range of pressures and temperatures.

Author contributions

R.J.M guided the research, C.R. performed the pulse experiments and kinetic modelling. M.L. performed the flow reactor experiments. R.M and C.R. wrote the manuscript.

Competing interests

The authors declare no competing interests.

Supporting Information

The supporting information contains information on the DOSC calculation (Figure S1), experimentally measured selectivities for varying inlet reactant pressures (Figure S2), Degree of Selectivity control contour plots for CO_2 (Figure S3), and the Degree of Rate Control contour plots for all three products (Figures S4 – S6). This information is available free of charge on the ACS Publications website.

Acknowledgements

This work was supported as part of the Integrated Mesoscale Architectures for Sustainable Catalysis (IMASC), an Energy Frontier Research Center funded by the U.S. Department of Energy, Office of Science, Basic Energy Sciences under Award #DE-SC0012573

References

(1) WACHS, I. The Selective Oxidation of CH3OH to H2CO on a Copper(110) Catalyst. *J. Catal.* **1978**, *53* (2), 208–227.

(2) Wachs, I. E.; Madix, R. J. The Oxidation of Methanol on a Silver (110) Catalyst. *Surf. Sci.* **1978**, *76* (2), 531–558.

(3) Gleaves, J. T.; Ebner, J. R.; Kuechler, T. C. Temporal Analysis of Products (TAP)—A Unique Catalyst Evaluation System with Submillisecond Time Resolution. *Catal. Rev.* **1988**, *30* (1), 49–116.

(4) Gleaves, J. J. T.; Yablonskii, G. G. S.; Phanawadee, P.; Schuurman, Y. TAP-2: An Interrogative Kinetics Approach. *Appl. Catal. A.* **1997**; 160 (1), 55–88.

(5) Reece, C.; Redekop, E. A.; Karakalos, S.; Friend, C. M.; Madix, R. J. Crossing the Great Divide between Single-Crystal Reactivity and Actual Catalyst Selectivity with Pressure Transients. *Nat. Catal.* **2018**, *1* (11), 852–859.

(6) Xu, B.; Friend, C. M. Oxidative Coupling of Alcohols on Gold: Insights from Experiments and Theory. *Faraday Discuss.* **2011**, *152*, 307.

(7) Xu, B.; Madix, R. J.; Friend, C. M. Achieving Optimum Selectivity in Oxygen Assisted Alcohol Cross-Coupling on Gold. *J. Am. Chem. Soc.* **2010**, *132* (46), 16571–16580.

(8) Xu, B.; Liu, X.; Haubrich, J.; Madix, R. J.; Friend, C. M. Selectivity Control in Gold-

Mediated Esterification of Methanol. *Angew. Chemie - Int. Ed.* **2009**, *48* (23), 4206–4209.

(9) Xu, B.; Madix, R. J.; Friend, C. M. Predicting Gold-Mediated Catalytic Oxidative-Coupling Reactions from Single Crystal Studies. *Acc. Chem. Res.* **2014**, *47* (3), 761–772.

(10) Stowers, K. J.; Madix, R. J.; Friend, C. M. From Model Studies on Au(111) to Working Conditions with Unsupported Nanoporous Gold Catalysts: Oxygen-Assisted Coupling Reactions. *J. Catal.* **2013**, *308* (December), 131–141.

(11) Personick, M. L.; Zugic, B.; Biener, M. M.; Biener, J.; Madix, R. J.; Friend, C. M. Ozone-Activated Nanoporous Gold: A Stable and Storable Material for Catalytic Oxidation. *ACS Catal.* **2015**, *5* (7), 4237–4241.

(12) Wittstock, A.; Zielasek, V.; Biener, J.; Friend, C. M.; Bäumer, M. Nanoporous Gold Catalysts for Selective Gas-Phase Oxidative Coupling of Methanol at Low Temperature. *Science* **2010**, *327* (5963), 319–322.

(13) Zugic, B.; Wang, L.; Heine, C.; Zakharov, D. N.; Lechner, B. A. J.; Stach, E. A.; Biener, J.; Salmeron, M.; Madix, R. J.; Friend, C. M. Dynamic Restructuring Drives Catalytic Activity on Nanoporous Gold–silver Alloy Catalysts. *Nat. Mater.* **2016**, *16* (5), 558–564.

(14) Wittstock, A.; Neumann, B.; Schaefer, A.; Dumbuya, K.; Kübel, C.; Biener, M. M.; Zielasek, V.; Steinrück, H.-P.; Gottfried, J. M.; Biener, J. Hazma, A.; Bäumer, M. Nanoporous Au: An Unsupported Pure Gold Catalyst? *J. Phys. Chem. C* **2009**, *113* (14), 5593–5600.

(15) Shekhtman, S. O.; Yablonsky, G. S.; Chen, S.; Gleaves, J. T. Thin-Zone TAP-Reactor--Theory and Application. *Chem. Eng. Sci.* **1999**, *54* (20), 4371–4378.

(16) Constales, D.; Yablonsky, G. S.; Marin, G. B.; Gleaves, J. T. Multi-Zone TAP-Reactors Theory and Application: I. The Global Transfer Matrix Equation. *Chem. Eng. Sci.* **2001**, *56* (1), 133–149.

(17) Gleaves, J. T.; Yablonsky, G.; Zheng, X.; Fushimi, R.; Mills, P. L. Temporal Analysis of Products (TAP)—recent Advances in Technology for Kinetic Analysis of Multi-Component Catalysts. *J. Mol. Catal. A Chem.* **2010**, *315* (2), 108–134.

(18) Schuurman, Y. Assessment of Kinetic Modeling Procedures of TAP Experiments. *Catal. Today* **2007**, *121* (3–4), 187–196.

(19) Yablonsky, G. S.; Olea, M.; Marin, G. B. Temporal Analysis of Products: Basic Principles, Applications, and Theory. *J. Catal.* **2003**, *216* (1), 120–134.

(20) The Mathworks Inc. MATLAB - MathWorks http://www.mathworks.com/products/matlab/.

(21) Shampine, L. F.; Reichelt, M. W. The MATLAB ODE Suite. *SIAM J. Sci. Comput.* **1997**, *18* (1), 1–22.

(22) Neurock, M. The Microkinetics of Heterogeneous Catalysis. By J. A. Dumesic, D. F. Rudd, L. M. Aparicio, J. E. Rekoske, and A. A. Treviño, ACS Professional Reference Book, American Chemical Society, Washington, DC, 1993, 315 Pp. *AIChE J.* **1994**, *40* (6), 1085–1087.

(23) Wang, L.-C.; Friend, C. M.; Fushimi, R.; Madix, R. J. Active Site Densities, Oxygen Activation and Adsorbed Reactive Oxygen in Alcohol Activation on NpAu Catalysts. *Faraday Discuss.* **2016**, *188*, 57–67.

(24) Wang, L.-C.; Personick, M. L.; Karakalos, S.; Fushimi, R.; Friend, C. M.; Madix, R. J. Active Sites for Methanol Partial Oxidation on Nanoporous Gold Catalysts. *J. Catal.* **2016**, *344*, 778–783.

(25) Outka, D. A.; Madix, R. J. Acid-Base and Nucleophilic Chemistry of Atomic Oxygen on the Au(110) Surface: Reactions with Formic Acid and Formaldehyde. *Surf. Sci.* **1987**, *179* (2–3), 361–376.

(26) Campbell, C. T.; Árnadóttir, L.; Sellers, J. R. V. Kinetic Prefactors of Reactions on Solid Surfaces. *Zeitschrift für Phys. Chemie* **2013**, *227* (9–11), 1435-1454.

(27) Campbell, C. T. The Degree of Rate Control: A Powerful Tool for Catalysis Research. *ACS Catal.* **2017**, *7* (4), 2770–2779.

(28) Laidler, K. J. Rate Controlling Step: A Necessary or Useful Concept? *J. Chem. Educ.* **1988**, *65* (3), 250.

(29) Kosuda, K. M.; Wittstock, A.; Friend, C. M.; Bäumer, M. Oxygen-Mediated Coupling of Alcohols over Nanoporous Gold Catalysts at Ambient Pressures. *Angew. Chemie - Int. Ed.* **2012**, *51* (7), 1698–1701.

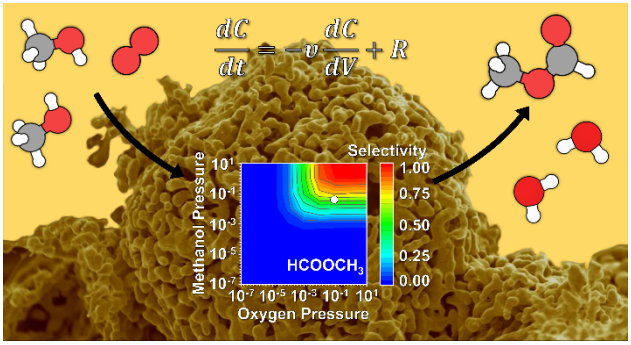

For Table of Contents Only